Magnetic Resonance Technology

A New Concept for Multiphase Flow Measurement

Jankees Hogendoorn (Krohne), André Boer (Krohne),
Matthias Appel (Shell), Hilko de Jong (Shell) and Rick de Leeuw (Shell).

---

1. Introduction

This paper describes a magnetic resonance based multiphase flow meter. During the last decades, magnetic resonance technology has enabled many industrial applications. One of the most well-known developments can be found in medical imaging. High resolution, three dimensional body scans can provide crucial information for medical diagnosis with many innovations being published every year. Another important field of application is the oil and gas industry. For many years, magnetic resonance based logging tools have been successfully used for detailed formation evaluation[1]. A scan of the vicinity of the bore hole provides important information about the reservoir rock structure and saturation condition with pore fluids, which is very important for oil production optimization.

Magnetic Resonance (MR) has specific advantages that can be used for multiphase flow measurement as well. A motivation of these advantages is presented in this paper. After a brief explanation of the principle of MR, a description is given how this principle has been applied in a multiphase flow meter. The conceptual design of the MR-based flow meter has been published previously[2] [3]. Significant efforts have been made to translate the conceptual prototype to an industrial design that meets oil-field requirements and specifications. A detailed description of this design is given in this paper too.

Finally, this paper summarizes the experimental and calibration results obtained during three-phase testing in an industrial flow loop. Magnetic resonance has been proven to have a lot of diagnostic capabilities in addition to flow quantification. Some of these capabilities are addressed at the end of this paper.

The paper finishes with a summary and conclusions.

2. The Challenge of Multiphase Flow Metering

Multiphase and wet gas flow meters provide essential online and continuous flow rate information in upstream oil and gas production systems[4]. During the last years, the associated technology has been matured such that acceptable performance can be achieved over a range of flow conditions. Nevertheless, a number of limitations persist and several specific requirements have not been adequately addressed by existing technologies. A couple of these limitations are listed below:

Meter hardware

- Most existing meters make use of gamma ray absorption technology for fluid identification. There is a strong industry desire to have a multiphase meter without radioactive sources.
- Many existing meters utilize differential pressure measurement, which, due to the quadratic dependence to flow rate, typically limits the dynamic range of the flow meter. This limitation often reduces the long-term applicability of a particular flow meter since

well production can vary considerably. Consequently, a flow meter that does not depend on the measurement of differential pressure would have advantages.
- Related to the previous item, a full-bore design is preferred in order to minimize the pressure loss created by the flow meter.

Technology
- Most multiphase flow meters require a priori knowledge of fluid properties at line conditions. Typical examples are individual fluid phase densities, gamma ray absorption coefficients and permittivity. These properties are difficult to predict without fluid samples. In addition, it is often impractical or even impossible to fill a flow meter with 100% of each fluid phase after field installation. MR technology offers the possibility to determine the required magnetic fluid properties with an un-separated fluid mix present in the meter.

Application needs
- At high Water Liquid Ratio (WLR), the uncertainty in the net oil rate measurement increases exponentially. For many oil field metering applications, there is a requirement for reducing the uncertainty in the high water liquid ratio region.
- High viscosity multiphase measurement is an additional challenge for existing technologies as it typically requires a number of additional assumptions and correlations, for example such as the Venturi meter discharge coefficient (Cd) as function of multiphase Reynolds number, bulk viscosity of oil/water emulsions, bulk liquid permittivity models, and updated slip models to mention a few.
- Adequate interpretation of flow meter data typically requires knowledge of the flow models and closure correlations (i.e. slip models, permittivity mixture rules, etc.) applied. However, the models and assumptions are typically proprietary for a particular flow meter manufacturer. Therefore, a more direct, less model-dependent measurement of individual phase velocities would be desirable.

3. Principles of Magnetic Resonance

By using the principle of Magnetic Resonance (MR), experiments are performed on the nuclei of atoms, by exposing them to a strong magnetic field. The strength of the magnetic field used in this technology depends on the application involved. Chemical applications utilize magnetic field strengths that are up to one million times stronger than the Earth's magnetic field measured at the equator. The magnetic field applied in the flow meter prototype described in this paper is approximately a thousand times stronger than the Earth's magnetic field.

MR is a consequence of the intrinsic magnetic moment of protons and neutrons. For most atoms, such as ^{12}C and ^{16}O, the individual magnetic moments of protons and neutrons offset each other, and the effective magnetic moment of such nuclei vanishes. Those atoms are invisible to MR. Other nuclei possess either an odd number of protons (^{1}H), or neutrons (^{13}C), or both protons and neutrons (^{2}H). If those atoms or isotopes have a sufficiently high natural abundance, they can be utilized in MR experiments. Hydrogen protons (^{1}H) (figure 1) provide the strongest MR response and are targeted in most oil-field applications of magnetic resonance[5] [6].

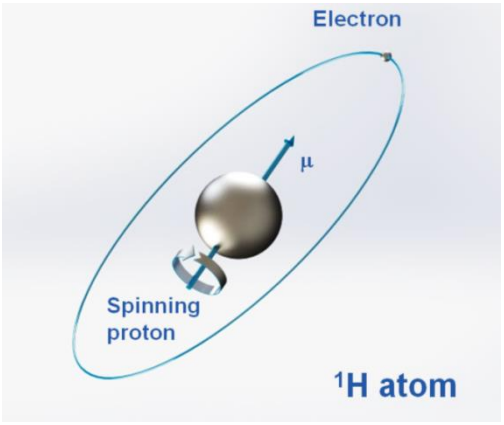

Figure 1 ^1H atom. The atom consists of a proton and an electron. The spinning proton has a magnetic moment, μ.

Precession / Resonance frequency

Similar to bar magnets, when a magnetic nucleus is placed between the poles of an external magnet, it too will try to align itself with respect to the externally applied magnetic field. The static magnetic field exerts a torque on the axis of the spinning magnetic moments, which, in turn, causes the axis to move perpendicular to the direction of the applied torque, and, hence, around the direction of the background magnetic field (figure 2). This motion is referred to as Larmor precession and is analogous to the motion of a spinning top in the Earth's gravitational field.

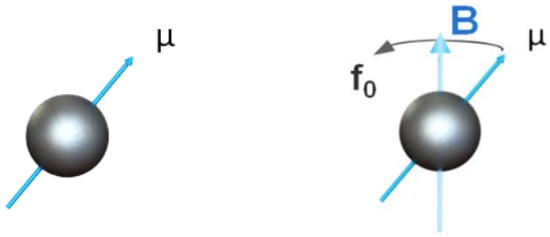

Figure 2 ^1H proton. Left-hand figure: no external static magnetic field. Right-hand figure: with external static magnetic field; the ^1H proton starts to precess along the magnetic field direction with the resonance (Larmor) frequency f_0.

The Larmor frequency, f_0, of this precession around the direction of the background magnetic field, $\vec{B}_0$, is determined by the gyromagnetic ratio, γ:

$$f_0 = -\frac{\gamma}{2\pi}\left|\vec{B}_0\right| \quad . \qquad (1)$$

The gyromagnetic ratio is a material constant. Commercial logging tools, as well as the magnetic resonance flow meter prototype, utilize permanent magnets of such strength that aligned protons precess with frequencies between several hundreds of kHz to a few MHz.

Magnetization

In the macroscopic world, magnets can be aligned in an infinite number of orientations (figure 3, left-hand figure). At the atomic level, however, only distinct alignments of the nuclei relative to the direction of an external magnetic field (also called spin states) are possible (figure 3, right-hand side). That is because direction and magnitude of the angular momentum of a nucleus, $\vec{I}$, are quantized, i.e., they can only vary by integer multiples of $\hbar$ (Planck's constant, h, divided by 2π).

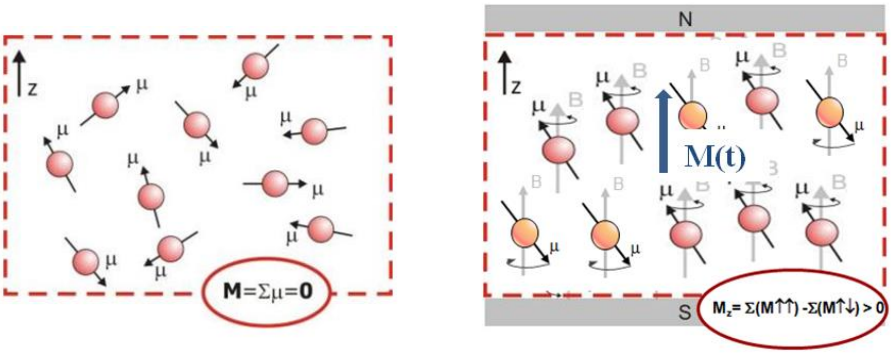

Figure 3 Left-hand figure: no external magnetic field; random orientation of protons, no net magnetization. Right-hand figure: external magnetic field; protons start to precess with the Larmor frequency. Net magnetization build up. The growth of the net magnetization (M) in time is referred to as the longitudinal relaxation (T_1).

For ^{1}H, two distinct alignments are possible. The nuclei can be aligned at a certain angle either with or against the external magnetic field. The population ratio of these two spin states is given approximately by the ratio of magnetic to thermal energy: at room temperature, there is approximately the same number of proton nuclei aligned with the main magnetic field as counter aligned. The aligned position is slightly favored, as the nucleus is at a lower energy state in this position. For every one million nuclei, there is about one extra nucleus aligned with the $\vec{B}_0$ field as opposed to the field. This phenomenon creates a net or macroscopic magnetization, in this paper subsequently referred to as $\vec{M}$, pointing in the direction of the main magnetic field (z-direction). This is illustrated in the right-hand picture of figure 3.

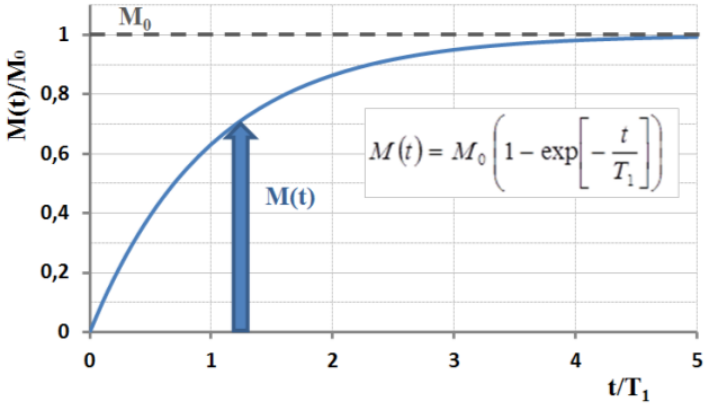

Figure 4 Time-dependent magnetization build-up. For a single-phase fluid, the magnetization builds-up exponentially and can be characterized by the so-called longitudinal relaxation time, T_1.

The magnetization build-up is time-dependent. For a single fluid, this build-up of magnetization can be characterized by a time constant called longitudinal relaxation time, T_1, as shown in figure 4. For mixtures of fluids, or more complex fluids, the magnetization build-up is typically characterized by a spectrum of longitudinal relaxation times. Short T_1-times result in fast magnetization build up.

Radio-Frequency pulses

The alignment of magnetic moments can be disturbed by radio-frequency (RF) pulses transmitted from an antenna to the fluids measured with the device (figure 5, left-hand figure). As a consequence, the orientation of the macroscopic magnetization, $\vec{M}$, can be modified by applying radio-frequency pulses with the appropriate intensity, duration, and frequency. Changes in the orientation or intensity of the macroscopic magnetization can be detected as a small voltage in an appropriate RF coil. It is this voltage which is measured as the MR signal in magnetic resonance experiments (figure 5).

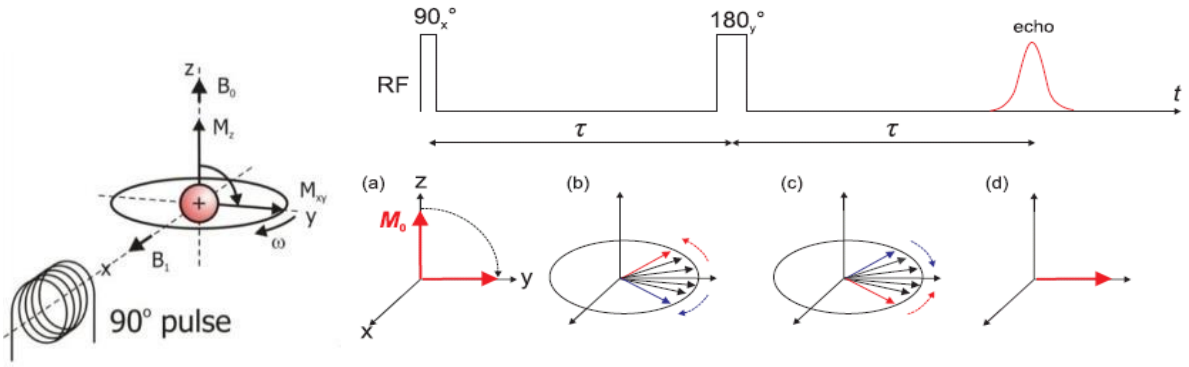

Figure 5 Hahn echo experiment. Left-hand figure: A P90 RF pulse flips the magnetization vector M_z in the horizontal xy-plane. Right-hand figure: a) P90 pulse b) de-phasing signal mainly due to differences in the local magnetic field, c) re-phasing signal after P180 pulse at $t=\tau$, d) echo at $t=2\tau$.

Hahn-echo

A well-known pulse experiment is the so-called Hahn-echo (spin-echo) experiment[5]. An RF pulse is created with the intensity and duration such that the magnetization vector, $\vec{M}$, is tilted along the x-axis by 90° (from the z-orientation to the xy-plane). This pulse is called a P90 pulse. After this pulse, the magnetization vector is rotating with the Larmor frequency in the xy-plane. However, due to spatial inhomogeneity in the magnetic field strength (leading to slightly differing Larmor frequencies of protons located in different positions), some protons lag behind and others move ahead during their Larmor precession. This is illustrated in figure 5b. As a consequence, the phase coherence slowly disappears, which, in turn, diminishes the magnetization vector and leads to a fast decaying signal. By applying a P180 pulse at $t=\tau$, all protons are flipped along the y-axis by 180°. As a result, the slower moving protons are placed ahead and the faster moving protons are placed behind. Since the individual resonance frequency is unchanged, all protons start to re-phase (figure 5c), leading to an echo at $t=2\tau$ (figure 5d). This echo is called the Hahn echo.

CPMG pulse sequence

Hahn echoes can be created multiple times by repeatedly applying P180 pulses. This pulse sequence is called the CPMG pulse sequence and is illustrated in figure 6. The name CPMG stands for the inventors of this sequence: Carr, Purcell, Meiboom and Gill[6]. By varying the time delay between subsequent P180 pulses, TE, different physical and chemical processes can be studied. Inter-echo spacings between tens or hundreds of microseconds to several milliseconds are typically applied during the CPMG sequence. Measuring several thousand echoes in one run is not uncommon.

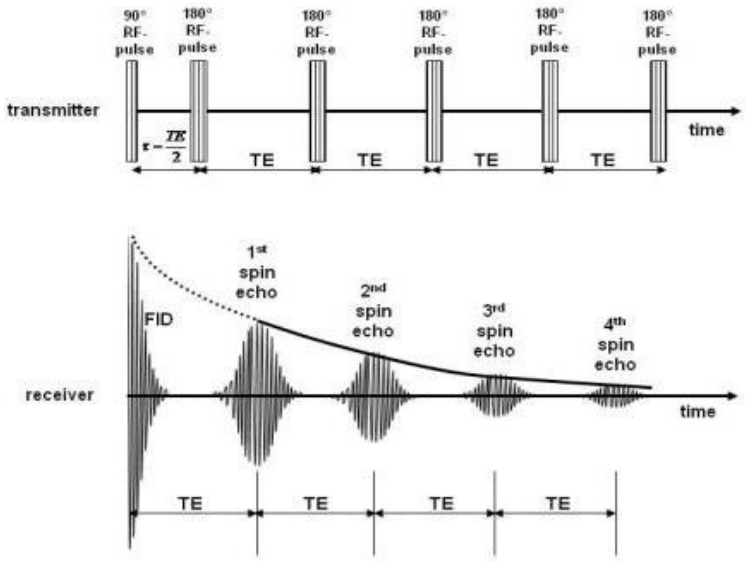

Figure 6 Illustration of the CPMG pulse sequence, creating multiple echoes.

During a CPMG sequence, the amplitudes of succeeding echoes are slightly attenuated relative to the previous echo because the reversal of the direction of the Larmor precession by a P180 pulse does not perfectly compensate for differences in the Larmor frequencies of different spins. Therefore, the signal envelope of all echoes acquired during the CPMG sequence eventually decays to noise level. This signal decay describes the return of the magnetic moments to their equilibrium state prior to the disturbance by RF pulses and is characterized by the so-called transverse relaxation time, T_2. This is shown in figure 7.

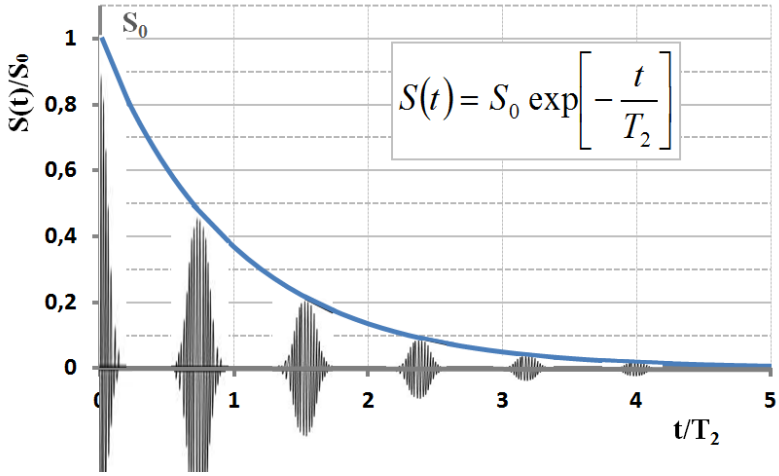

Figure 7 The decay of the spin echoes (blue line) is characterized by the transverse relaxation time, T_2.

In weak, homogenous magnetic fields, and for simple, symmetric molecules, the T_1- and T_2-relaxation times of fluids are similar, since both are governed by the molecular structure of the fluid (such as inter- and intra-molecular distances between the hydrogen atoms) as well as the ratio of viscosity to temperature[7].

Besides CPMG, a variety of RF pulse sequences have been developed for measuring T_1 or T_2. By varying the timing of these pulse sequences, the measurement can be optimized to the expected MR response of the flowing fluids.

Magnetization level

The intensity of the measured MR signal is determined by the magnitude of the macroscopic magnetization, $\left|\vec{M}\right|$, that has been created by the aligned molecular moments in the zone of investigation of the magnet. According to Curie's Law [8],

$$\vec{M} = N\frac{\gamma^2\hbar^2 I(I+1)}{3k_B T}\vec{B}_0 \quad . \qquad (2)$$

In this equation, I symbolizes the magnitude of the angular momentum (spin quantum number). To date, all oil-field MR applications exploit the magnetic resonance effect of protons (^{1}H), i.e., the magnetic moments in resonance are the hydrogen atoms associated with hydrocarbon and brine molecules. The spin quantum number of protons is ½. Finally, k_B represents Boltzmann's constant and T is absolute temperature. Equation 2 shows that the magnetization (and, hence, the intensity of the measured MR signal) is directly proportional to the number of magnetic moments (spins), N, that are in resonance with the operating frequency of the magnetic resonance device.

In order to determine fluid volumes from the measured MR signal, the number of magnetic moments sensed by the magnetic resonance device needs to be related to fluid volume. This is achieved by calibrating the MR device first to water at standard pressure and temperature conditions, and subsequently to determine the required correction for differences in the number of magnetic moments per unit volume between water and the measured fluid. This correction is referred to as a hydrogen index correction. The derivation of hydrogen indices for reservoir fluids has been extensively discussed in a variety of articles (e.g. [9]).

4. Magnetic Resonance for Multiphase Flow Measurement

Conceptually, a magnetic resonance experiment usually consists of three sequential steps:

1. Creating a net magnetization by aligning the magnetic moments of hydrogen atoms in an applied, constant magnetic field B_0.
2. Perturbing the alignment of hydrogen atoms by employing electro-magnetic radio frequency (RF) pulses.
3. Detecting the radio-frequency signal emitted by the hydrogen atoms during their return to equilibrium alignment in the external magnetic field.

This measurement principle also forms the basis of magnetic resonance based flow metering [2][3].

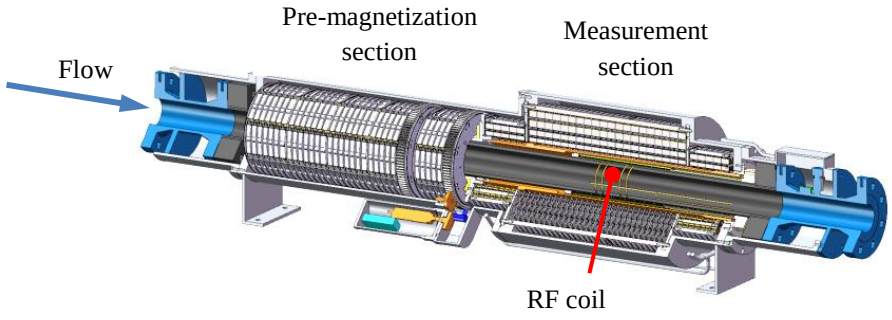

Figure 8 Simplified drawing of the magnetic resonance multiphase flow meter. The flow meter comprises two major components: the pre-magnetization section and the measurement section.

The flow meter comprises two major components: a pre-magnetization section and a perturbation and measurement section involving a radio-frequency coil (figure 8).

Pre-magnetization section – Water Liquid Ratio determination

In the pre-magnetization section, the hydrogen atoms are magnetized and a net macroscopic magnetization is created. Figure 4 shows the magnetization of the protons as function of time. In the flow meter, magnetization as function time can be transformed to magnetization as function of distance to the start of the pre-magnetization section by substituting the simple relation $t=x/v$ where x is the position within the pre-magnetization section and v is the flow velocity. The magnetization as function of x for a specific velocity and longitudinal relaxation time, T_1, is shown in figure 9.

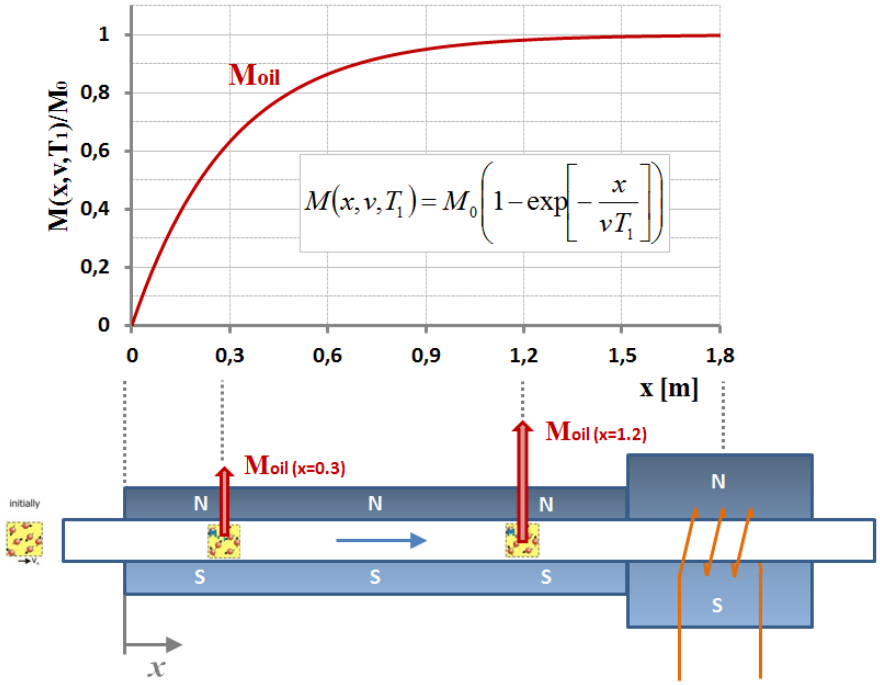

Figure 9 Magnetization build-up as a function of position inside the pre-magnetization section for a specific velocity and T_1. (v= 2[m/s], $T_{1\ oil}$ =0.15s).

An important property of oil and water, which is exploited in the MR multiphase flow meter, is the difference in longitudinal relaxation time, T_1. For most oil viscosities encountered in the industry, the longitudinal relaxation time, T_1, is significantly shorter than that of water. As a consequence, oil magnetizes faster than water (see figure 10, left-hand figure). This difference in the rate of magnetization build-up is used to create contrast between oil and water. By varying the effective length of the pre-magnetization section, the signals originating from oil and water, respectively, will be built-up to different levels, leading to quantitative information on the water-oil ratio. This process is illustrated in figure 10. In the left-hand figure, the full pre-magnetization length (labeled as configuration 111) is used. For the particular flow velocity displayed, this length is sufficient to achieve complete polarization of the oil signal, whereas the signal originating from water has been built up to approximately 30%. Consequently, the oil-water signal ratio ($S_{111oil}/S_{111water}$) in the measuring section adjacent to the pre-magnetization section is about 3. When the pre-magnetization length is reduced to just the length of the measuring section magnet (labeled as configuration 000), both the oil- and water signals are reduced but the signal from water is more strongly attenuated than the oil signal. This leads to an oil-water signal ratio ($S_{000oil}/S_{000water}$) of about 10 (right-hand side).

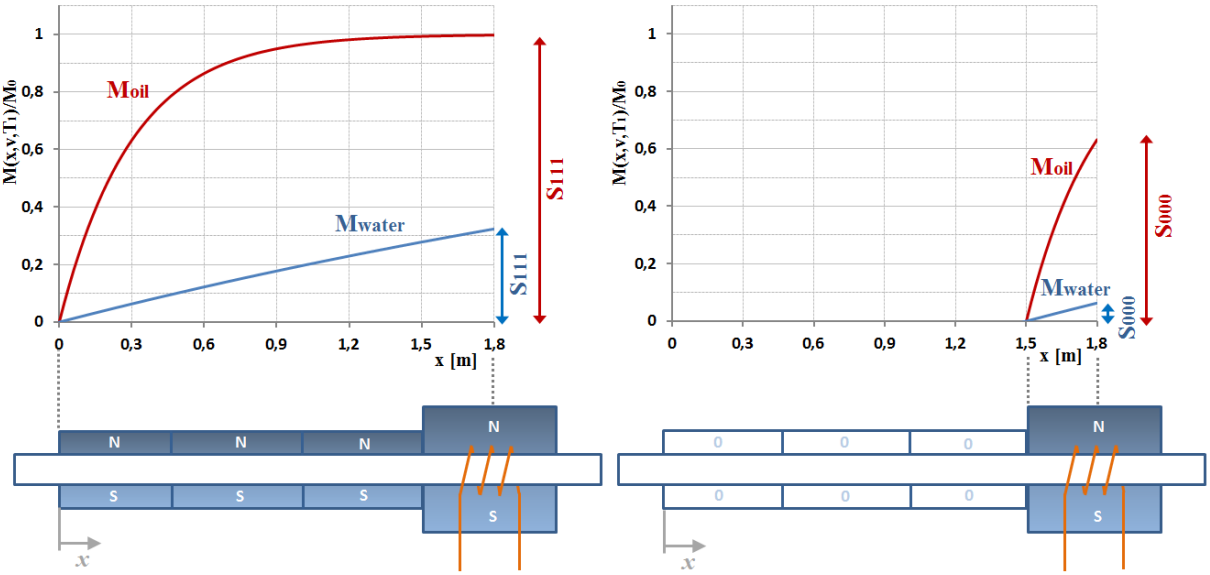

Figure 10 Build-up of magnetization and, hence, signal levels, for oil and water achieved with maximum pre-magnetization length (left-hand figure) and minimum pre-magnetization length (right-hand figure). The magnetization build-up has been calculated for a flow velocity, v, of 2 m/s and assuming longitudinal relaxation times, T_1, of 0.15 s and 2 s for oil and water, respectively.

Figure 10 demonstrates that a strong contrast can be created between the signals originating from oil and from water based on the difference in T_1 times by varying the pre-magnetization length. This contrast enables precise quantification of the oil-water ratio even for very high water liquid ratios. This capability is illustrated in figure 11. In this figure, the signal ratio S_{000}/S_{111} of both oil (red) and water (blue) are plotted as a function of flow velocity.

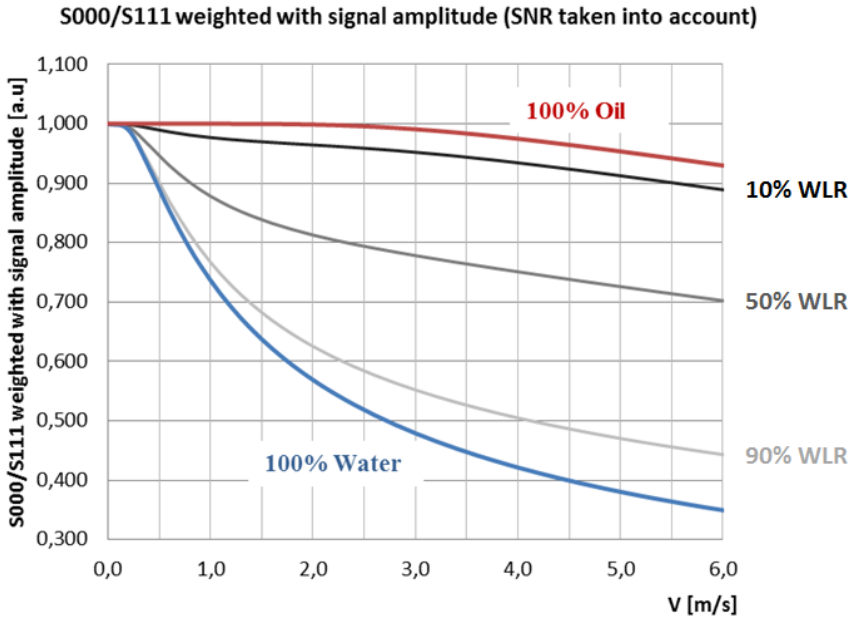

Figure 11 Signal ratio S_{000}/S_{111} as function of flow velocity for various oil-water ratios. The signal intensities have been calculated assuming longitudinal relaxation times of 0.15 s for oil and 2.3 s for water. A strong signal contrast between oil and water can be achieved even for high flow rates.

For multiphase flow of oil and water, the S_{000}/S_{111} curve will always fall between the pure oil and pure water curves. The shape of curves for different water liquid ratios can be calculated and has been added to figure 11 for water liquid ratios of 10%, 50% and 90%, respectively. Figure 10 also shows that the sensitivity of the MR flow meter for determining the water liquid ratio increases with increasing water liquid ratio, demonstrated by an increased separation of the water liquid ratio lines with increasing water liquid ratio. This method remains robust even when phase slip between the oil and water phases is present.

The water liquid ratio determination method is largely independent of the gas volume fraction (GVF) up to high GVF's because the gas signal is weak compared to the liquid signal. Once the gas fraction has been determined, as discussed in subsequent chapters, the gas signal can be subtracted from the respective signals S_{000} and S_{111}. This process produces liquid-only MR signals, which are used for water liquid ratio determination

Liquid velocity determination

The flow velocity is determined by using the so-called convective decay method. In the measurement section, the alignment of hydrogen atoms relative to the direction of the external magnetic field is perturbed by irradiating RF energy using a RF coil and a pre-defined pulse sequence, such as a CPMG sequence introduced earlier. The spin echoes produced by the sample are detected by the same RF coil also used for irradiating the RF energy. The amplitude of the initial Hahn echo has the highest value since all excited protons are still inside the RF coil. In contrast, when the second Hahn echo is formed about 1 ms later, a certain fraction of excited protons has already flown out of the RF coil. Consequently, the amplitude of the second echo will be somewhat lower than that of the first echo, even if there was no transverse relaxation. All following echoes are successively attenuated, since more and more protons that were excited by the initial RF pulse have left the RF coil. This 'convective decay' of the echo signals is shown in figure 12.

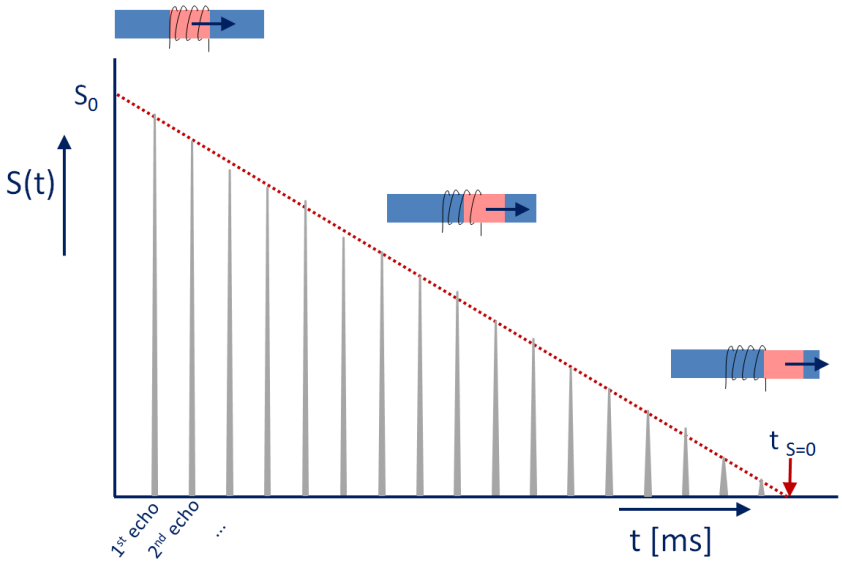

Figure 12 Velocity determination using the so-called convective decay method. Ignoring magnetic relaxation effects, the measured echo amplitude decreases linearly with time since the excited protons are leaving the RF coil due the flow. At a certain time all excited protons have left the RF coil. The RF coil length divided by the time at which the red dashed line intercepts the horizontal axis yields flow velocity.

The signal decay is proportional to the flow velocity. The higher the flow the faster the echo decay. The flow velocity is equal to the length of the RF coil, L_c (typically 10 cm), divided by the time at which the red dashed curve intercepts the x-axis, $t_{S=0}$, so $v = L_c/t_{S=0}$ [10].
Combining the convective decay method with varying the pre-magnetization length enables the direct measurement of velocity slip between the flowing liquid phases. As shown in figure 10, signal contrast can be created between water and oil by modifying the effective pre-magnetization length. For a long pre-magnetization length, the initial signal, S_0, in figure 12 is a composition of signal contributions originating from both oil and water.
The velocity that is obtained from the convective signal decay is a composition of the oil and water velocities. In contrast to this, the initial signal amplitude corresponds predominantly to oil if a short pre-magnetization length is selected, cf. figure 12. Consequently, the velocity that is being measured for this pre-magnetization configuration predominantly reflects the oil velocity. This, in combination with the measured water liquid ratio, makes it possible to determine both the oil and water velocities independently.

Gas volume fraction and gas velocity determination

The MR flow meter is capable of directly measuring the Gas Volume Fraction (GVF) and the gas phase velocity. However, as patents on this are still pending the background of this technique will not be further discussed in this paper.

5. Mechanical design of the MR multiphase flow meter

The current flow meter is operated in a horizontal configuration. The design is an industrialized version of the improved and tested prototype version and has a 4" 600lbs, full bore pipe. No specific upstream flow conditioning measures are required. The connecting flanges are made from stainless steel (SS) or carbon steel (CS). The overall flange-to-flange length is about 3m. Maximum process temperature is 100°C and the minimum and maximum ambient operating temperatures range from -40°C to +65°C. All electronics are mounted directly on the flow meter in two flame-proof boxes (see figure 13).

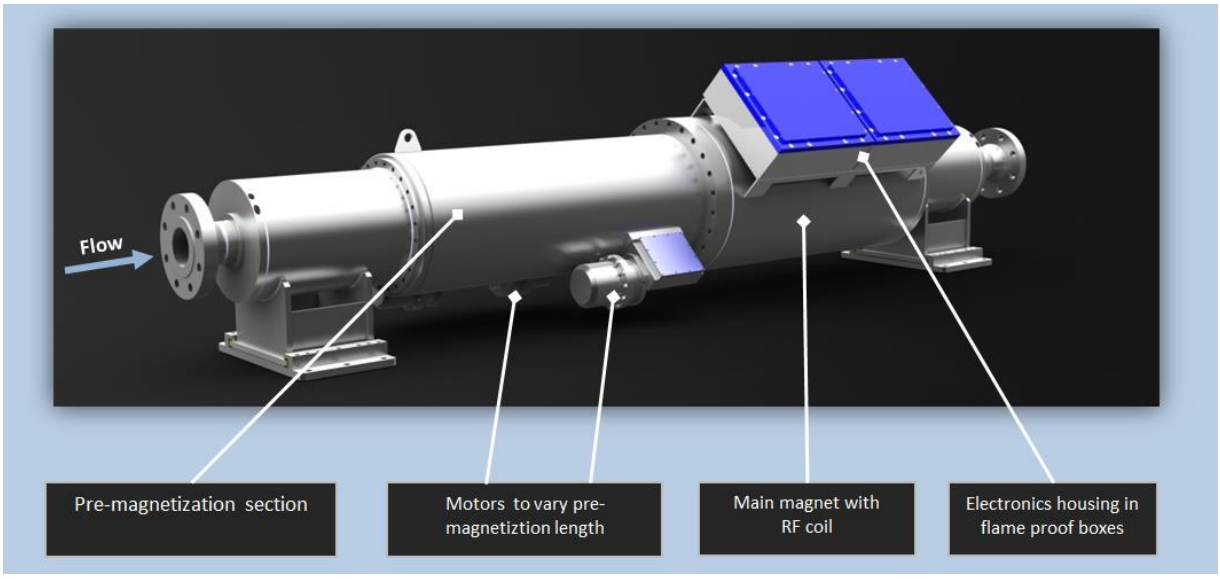

Figure 13 External mechanical design of the industrialized version of the MR multiphase flow meter. All electronics are mounted on the flow meter in explosion-safe boxes. The overall length is about 3 m.

Tube design

An important feature of the MR flow meter is that there are no protrusions into the pipe. Inside the flow meter, the transition is made from steel flanges to a glass fiber reinforced epoxy (GRE) pipe (see figure 14). A non-conductive pipe section is required to allow high frequency electromagnetic waves to be transmitted into the pipe. All measurements are made from outside of the tube. There is no feed-through or anything else puncturing the tube.

The selected GRE pipe and flanges are frequently used in the oil and gas industry and possess all required certifications and approvals. The forces from the connected piping system are guided through the external housing in order to prevent mechanical loading of the GRE pipe.

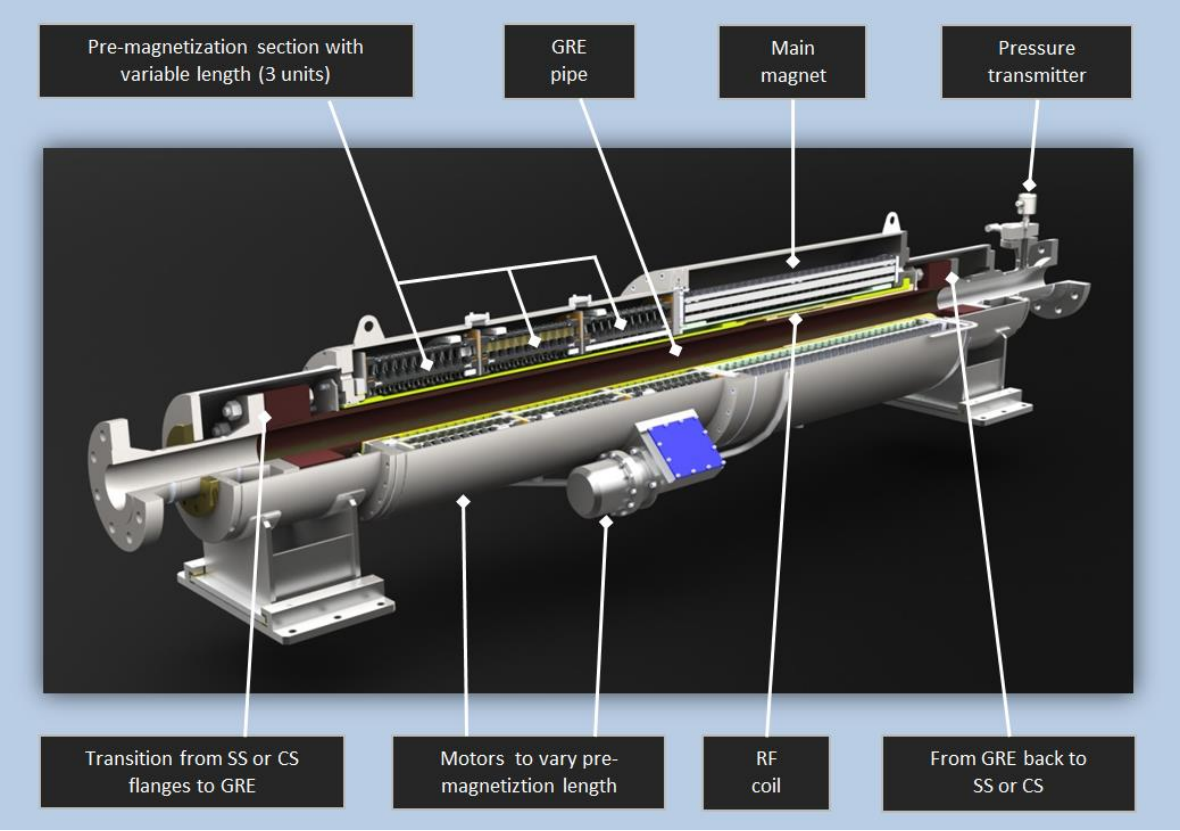

Figure 14 The internal mechanical design of the industrialized MR multiphase flow meter. The flow meter has a full bore design.

Pre-magnetization section

The pre-magnetization section consists of three individual pre-magnetization units. A pre-magnetization unit consists of two concentric rings; an inner and outer ring. The outer ring can be rotated around the inner ring using electro-motors. The magnetic field strengths of the outer and inner rings are equal. By putting both rings in the upward direction (+/+), full magnetic field strength is obtained. By rotating the outer ring by 180° (+/–) the magnetic field created by the inner ring is cancelled out by the outer ring. Each pre-magnetization section has one motor mounted in a flame-proof housing.

Main magnet – Measurement section

The magnetic field strength in the main magnet is equal to the magnetic field strength in the pre-magnetization section. However, the magnetic field homogeneity of the main magnet is orders of magnitude higher than the homogeneity of the pre-magnetization section. The high field homogeneity is necessary for proper proton resonance measurements.

In contrast to the magnetic field strength inside the pipe, the magnetic field strength outside the meter housing is very weak (< 0.5 mT). This level is below the maximum field strength legally specified by standards. The value 0.5 mT is about 10 times stronger than the Earth's magnetic field strength.
In between the main magnet and the GRE pipe, the radio frequency coil is located. The RF coil is transmitting and receiving the signals and is matched and tuned to the Larmor precession of flowing phases by a matching and tuning circuit mounted in the electronics housing.

Outlet section
In the outlet section, the GRE pipe is coupled to a SS or CS flange section. In the metal spool piece a pressure transmitter is mounted. This pressure transmitter can be replaced without depressurizing the system. The body temperature of the pipe section is measured on the outside of the metal spool piece inside the external housing. Thermal insulation makes sure that the temperature measurement is representative for the process fluid temperature.

6. Tests at commercial flow loop with improved prototype

Prototype versions of the magnetic resonance flow meter has been tested at a commercial flow loop located at the Southwest Research Institute multiphase test facility in San Antonio, Texas, USA, in February and March, 2013 (figure 15).

SwRI Test facility
The operation of the flow loop consists of a multiphase flow stream from a pump discharging into a separator where the flow components are divided into gas and oil and water streams that can be separately metered and routed to the test section. The liquid flow rate is measured with a Coriolis meter. Specified uncertainty is less than 0.5% at the high flow rates to around 1% at the lower flow rates.

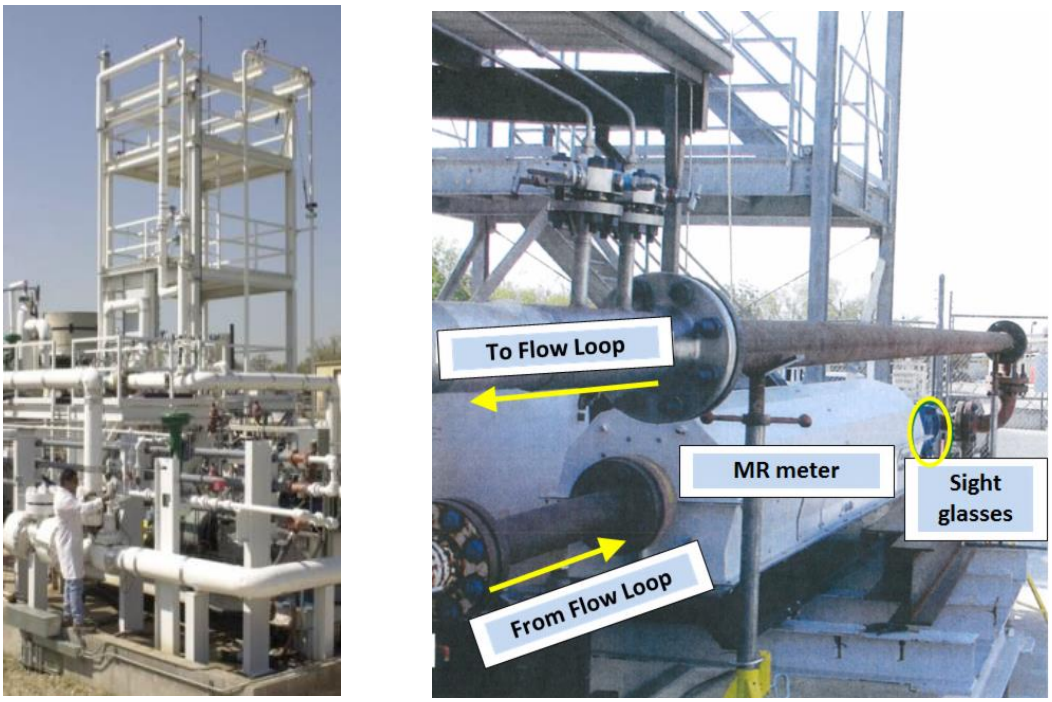

Figure 15 Tests with an improved prototype version of the magnetic resonance flow meter at the multiphase test loop of SwRI at San Antonio, February/March 2013.

The small amount of gas present in the liquid due to imperfect separation is measured with a separate device. The uncertainty of this GVF meter is 5% of reading.
The water liquid ratio of the liquid mixture was monitored through collection (figure 16) and the averaging of two liquid samples taken at each test point .

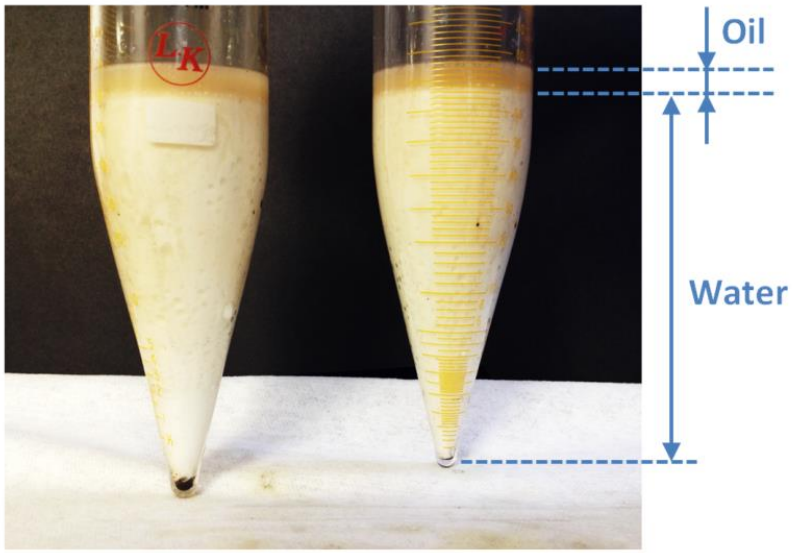

Figure 16 Manual water liquid ratio determination by means of samples.

The reference gas flow rate was measured using an orifice meter for the higher flow rates and a small bore (½") Coriolis meter for the lower flow rates (< 12 m3/h). The typical uncertainty specified for the dry gas orifice flow meter is 0.5 to 1.0% (dependent on the flow rate) and 0.35% for the Coriolis meter. Fresh water, oil (Regal R&O 32 VSI, viscosity about 43 cSt @ 32°C) and methane have been used as test fluids. The operating pressure and temperature was around 83 bar(g) bar(g) and 32°C respectively. The liquid flow rates have been varied from 0.64 to 46 m^3/h and the gas flow rate from 2 to 107 m^3/h in varying ratios (see table 1).

Test Conditions	**Range**
Static pressure, bar(g)	82.7
Temperature, °C	32
Liquid Flow Rate, m3/h	0.64 – 46.3
Gas Flow Rate, m3/h (actual)	2.0 – 107.0
GVF, %	0, 25, 50, 70, 90 and 100
Water liquid ratio, %	0, 30, 60, 80-95 and 100
Flow regimes	Single phase, stratified, stratified wavy, plug and slug flow

Table 1 Overview of the multiphase test conditions.

Tests at six different gas volume fractions (GVF) have been carried out: 0%, 25%, 50%, 70%, 90% and 100% (see figure 17).

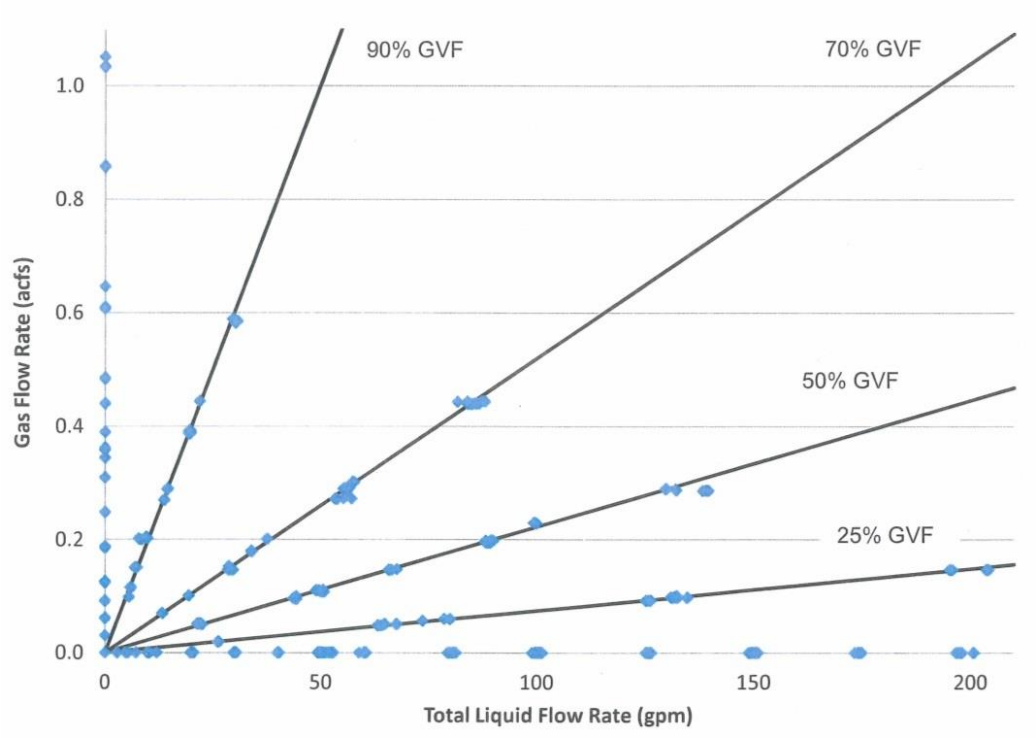

Figure 17 Gas flow versus total liquid flow at various gas volume fractions. A value of 1.0 actual cubic feet per second (acfs) corresponds to about 102 m^3/h. The value of 200 gallons per minute (gpm) corresponds to about 45.4 m^3/h.

The Water Liquid Ratio has been tested at 0%, 30%, 60%, 80%, 95% and 100%. Since it took significant time to precisely adjust the WLR to a certain desired value, the WLR test points in the range of 80 to 95% have been approximately set by the test loop operator. The WLR value as obtained was accepted without further adjustment. This procedure saved valuable test time. An overview of the test points for GVF versus WLR is given in figure 18.

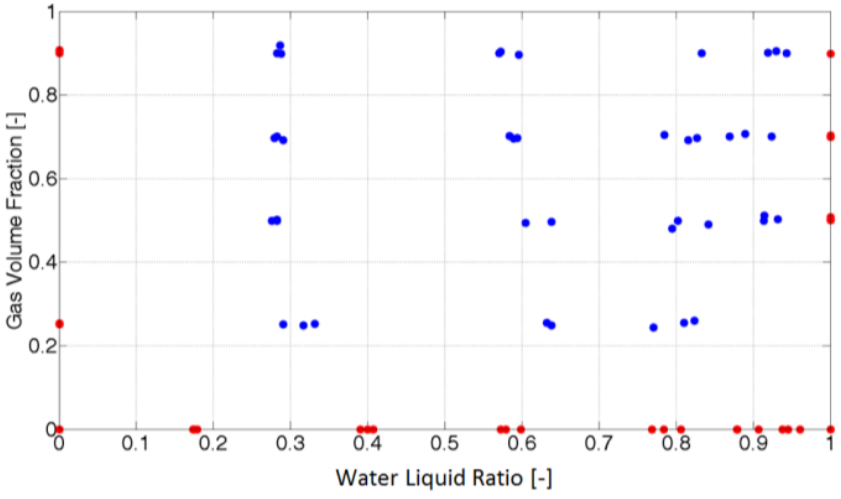

Figure 18 Test points plotted as gas volume fraction versus water liquid ratio. The blue dots indicate the three phase test points, the red dots are marking the two phase test conditions.

Test results

As an example, figure 19 shows the amplitudes of successive Hahn echoes as function of time during a CPMG sequence for a three phase flow situation (WLR=77%, superficial liquid velocity

1.64 m/s, superficial gas velocity 0.53 m/s, plug flow according flow map). By means of a linear fit through the data points the bulk flow velocity could be determined (as explained in figure 12).

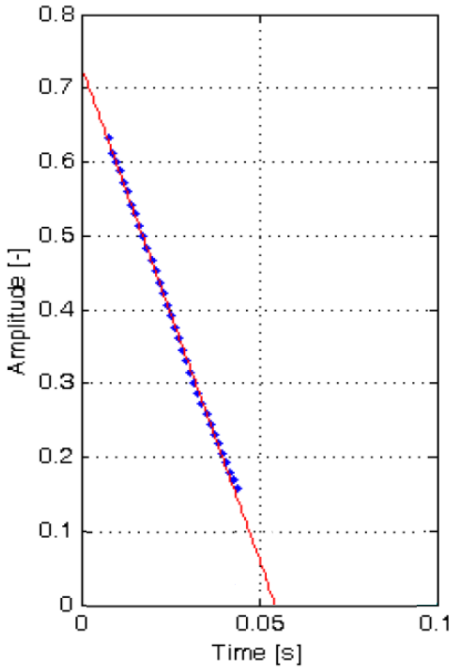

Figure 19 Echo amplitudes as function of time during a CPMG sequence for a three phase flow situation. WLR=77%, superficial liquid velocity: 1.64 m/s, superficial gas velocity 0.53 m/s (plug flow regime according flow map).On basis of the linear fit through the data points, the bulk velocity could be determined.

In chapter four, it has been explained that contrast between oil and water (which is used for water liquid ratio determination) can be created by exploiting differences in the magnetization build up associated with different pre-magnetization lengths. It is essential that the magnetization build-up corresponds to the theoretically predicted levels. Experimental and theoretical results are compared in figure 20. This figure shows the magnetization build-up for different pre-magnetization lengths as function of flow velocity. The signal with maximum pre-magnetization length is used to normalize the data. The symbols represent experimental data, whereas the solid lines display the curves predicted by theory. The left hand figure is the result of gas measurements, the right hand figure is an experiment on water.

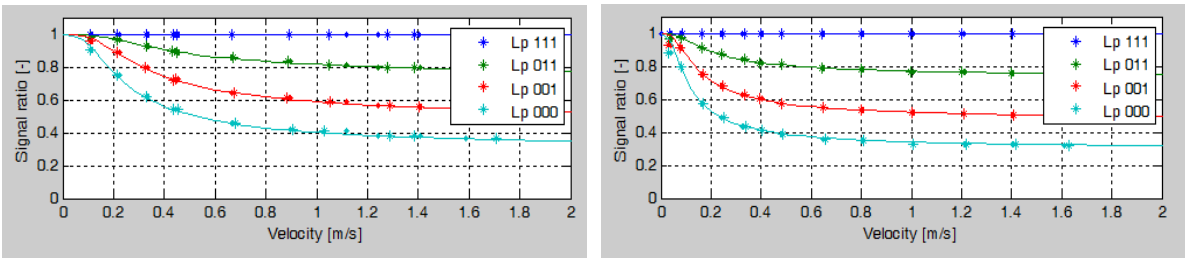

Figure 20 Magnetization build-up as function of velocity for different pre-magnetization lengths. The maximum pre-magnetization length (Lp111) has been taken to normalize the data. Left-hand figure: single phase gas, right-hand figure: single phase water. The symbols are experimental data, the solid lines are the curves predicted by theory.

A similar graph for a multiphase situation (*WLR=28%, GVF=50%.)* is shown in figure 21. This graph is comparable to figure 11. The dark blue line corresponds to single phase water (equal to

light blue line in figure 20 right-hand side), the red line corresponds to single phase oil. The blue dot represents the value that has been measured, leading to a WLR reading of 29%. The green line is the reference WLR value, which is equal to 28%.

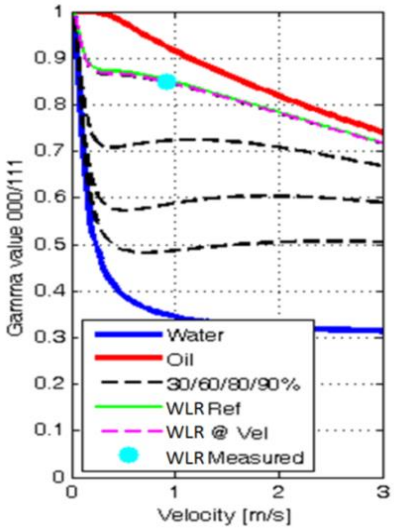

Figure 21 Signal ratio acquired with minimum and maximum pre-magnetization lengths, S_{000}/S_{111}, as function of flow velocity for various oil-water ratios. The blue dot represents the value that has been measured, leading to a WLR reading of 29%. The green line is the reference WLR value, which is equal to 28%. The GVF in this experiment was 50%.

Next to the WLR, the total liquid flow rate and the gas flow rate were determined. On the basis of these parameters, the GVF, oil flow rate and water flow rate were derived. Two examples of analysis are shown in figures 22 and 23.
Figure 22 (left-hand) shows the superficial gas and liquid velocities of both the reference and the MR multiphase flow meter. The right-hand figure shows the WLR versus the superficial liquid velocity for both the reference and the flow meter reading (WLR=28%, GVF=50%). Figure 23 is analogue to 22 but for a WLR of 92% and a GVF of 90%.

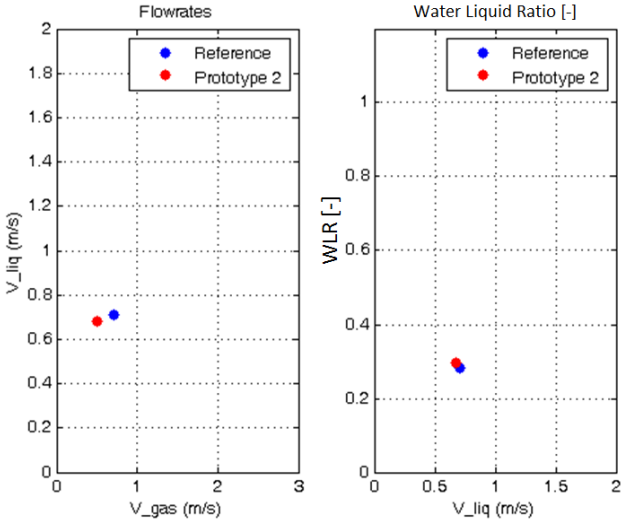

Figure 22 Superficial gas and liquid flow velocity (left-hand) and WLR versus superficial liquid velocity (right-hand). Both the reference and MR multiphase reading are shown. WLR=28%, GVF=50%.

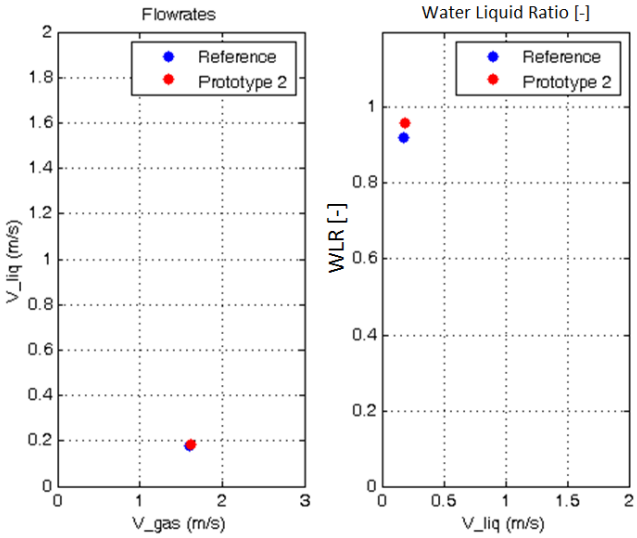

Figure 23 Superficial gas and liquid flow velocity (left-hand) and WLR versus superficial liquid velocity (right-hand). Both the reference and MR multiphase reading are shown. WLR=92%, GVF=90%.

This analysis has been carried out for all 41 multiphase test points. The results for the total liquid flow, gas flow, oil flow and water liquid ratio are shown as a cumulative performance plot[11] in figure 24. All 41 multiphase tests points have been included. In this graph we find the deviation between the reference and the MR multiphase flow meter on the x-axis, and the cumulative percentage of the test points that fulfill the deviation criteria on the y-axis. The full scale value is 2 m/s. This full scale value is based on the range tested.

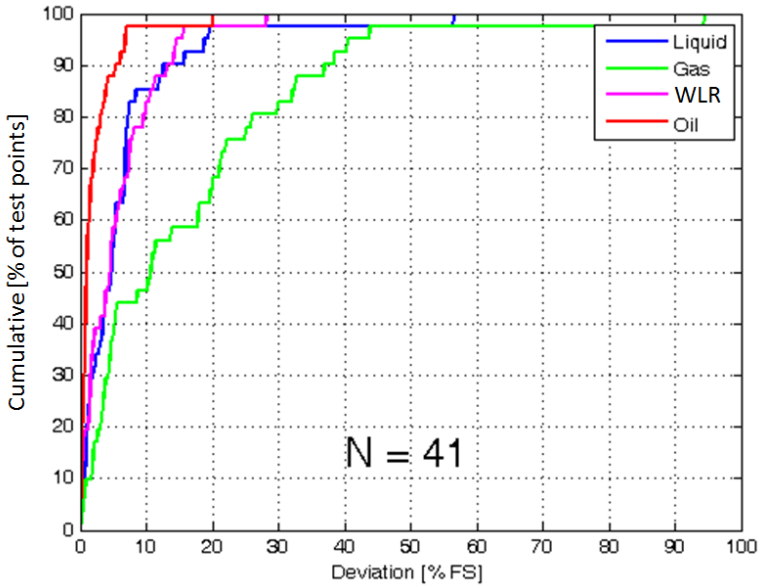

Figure 24 Results on total liquid flow, gas flow, oil flow and water liquid ratio shown in a cumulative performance plot. This plot provides the percentage of test points that show a particular deviation between experimental and reference data displayed on the x-axis. All three phase test points (N=41) are included in this graph.

A number of comments need to be made:

- For the gas flow measurements, a simplified interpretation model was used. This model has a number of known limitations. A new model is available, but was not implemented at

the time of testing the flow meter. Implementation of the new gas model will significantly improve the results.

- WLR: Analysis of these results provided us with input for further model improvement. Calculations indicate that a significant improvement in the accuracy of water liquid ratio determination can be expected too.
- Liquid flow: A similar improvement is expected for the determination of liquid flow rates.

In order to quantify the performance of the MR flow meter at different flow conditions, the data points, as shown in figure 24, could be split up in different quadrants; lower and higher WLR, lower and higher GVF. Preferably, a split in four different GVF ranges is made[11]. However, due to the limited number of data points, this would lead to statistically unreliable curves. For this reason the data set has been divided into two GVF ranges, a higher and lower GVF range with a division at GVF=75%. In the higher GVF range (10 experiments), all measurements on the different water liquid ratios are combined. The lower GVF range is split in three water liquid ratio ranges: an oil-continuous phase (0<WLR<50%), a transition zone (50%<WLR<85%), and a high water liquid ratio range (WLR>85%). The results are shown in figure 25.

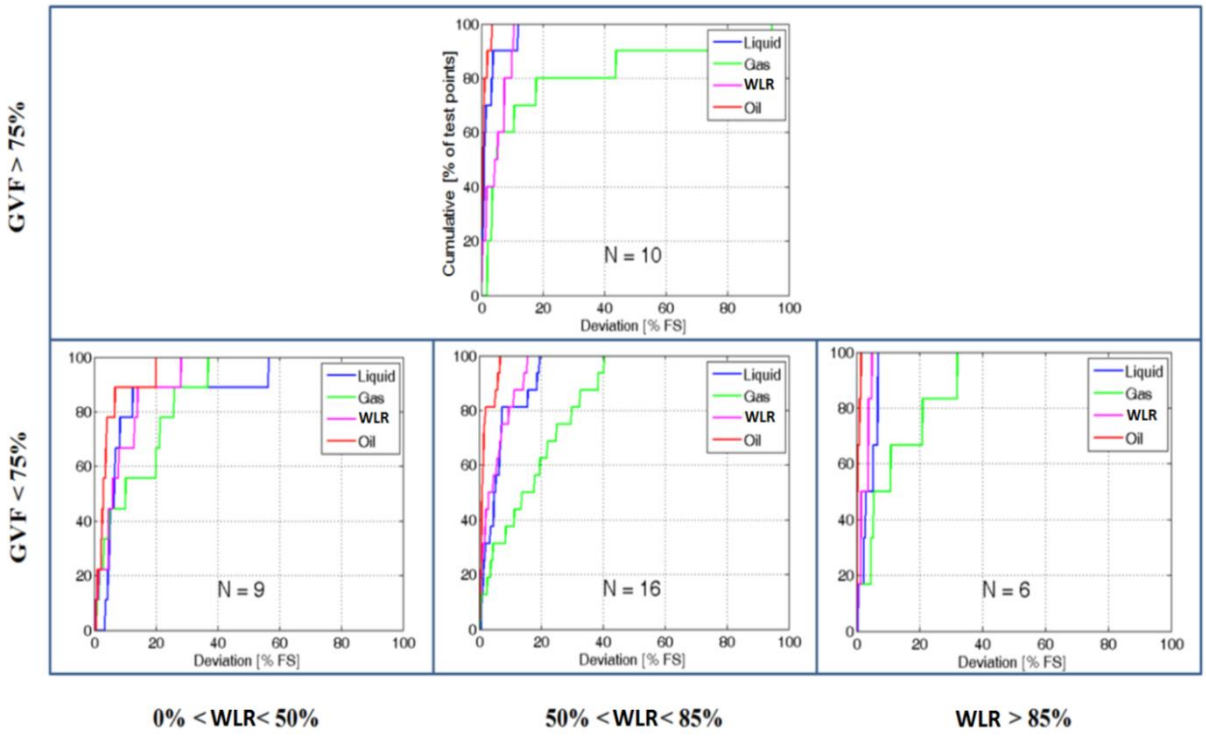

Figure 25 Results on total liquid flow, gas flow, oil flow and water liquid ratio shown in a cumulative performance plot, divided into four quadrants. The data set was divided at a GVF of 75%. For GVF>75% all test points are plotted in one graph; for GVF<75%, the test points are divided into three WLR ranges. The full scale value is 2 m/s.

On basis of these results, we observed that there is not a specific range in which the meter shows a particular weakness. At the same time, we observe an improved performance with increasing WLR. This corresponds to the expected performance as explained in figure 11, which shows an increasing sensitivity of the MR flow meter with increasing WLR. Consequently, based on the theoretical characterization of the MR flow meter and the extensive three-phase flow tests, the sweet spot of the meter was identified in the high WLR range at lower GVF's.

As mentioned before, analysis of the experiments should lead to significant model improvements. These improvements shall be implemented in the new industrialized version of the MR multiphase flow meter (shown in figures 13 and 14).

An industrialized version of the MR multiphase flow meter (see figure 26), as conceptually described in chapter 5, will be tested in various commercial flow loops in Q4, 2013. Following successful flow loop tests, a field test at a hydrocarbon production facility near Rotterdam, The Netherlands, has been scheduled. This oil field has a newly equipped test separator for providing reference data. The field trial will in addition test the field-robustness of the flow meter. The various wells in production offer a reasonable range of flow rates and water liquid ratios.

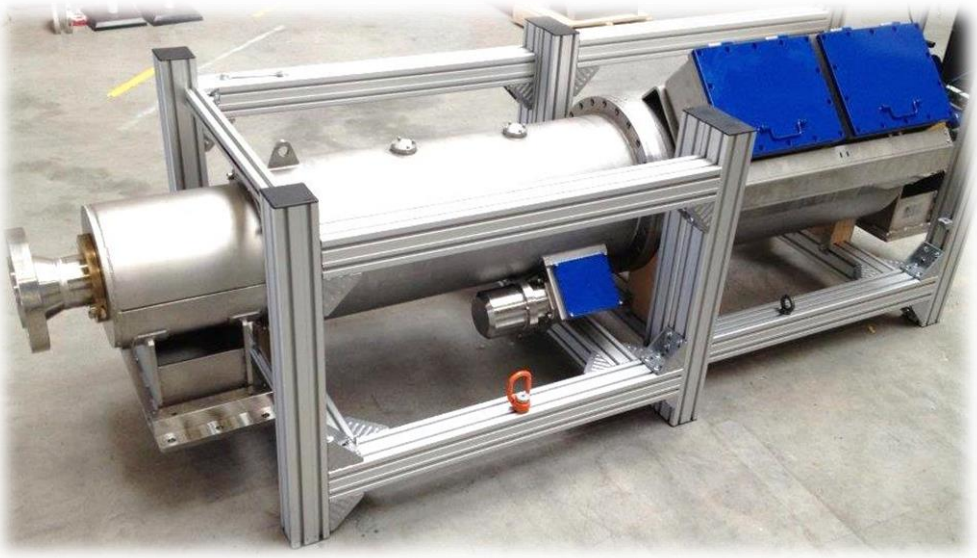

Figure 26 Picture of the industrialized version of the MR multiphase flow meter. The flow meter is mounted in a production frame that will be removed during installation.

7. Diagnostic capabilities and future potential

In addition to flow measurements, the MR multiphase flow meter has strong diagnostic capabilities. The matching and tuning of the electronic circuitry contains valuable information about the process conditions inside the tube. The same holds for the spin echo shape. Another example is the possibility to acquire a T_2 relaxation time spectrum analysis. An illustration is given in figure 27.
By using the data obtained as shown in figure 7, a T_2 relaxation time spectrum can be generated for either static fluids or if the flow velocities have been determined. As addressed earlier, the T_2 relaxation time is directly related to molecular structure. Figure 27 shows a spectrum of transverse relaxation time, T_2, which is generated from a bottle filled with approximately 70% air (no signal), 27% water and 3% oil. The composition of the synthetic oil was not known. The relaxation time spectrum shows a strong peak at about 2.2 s, which corresponds to the transverse relaxation expected for bulk water.

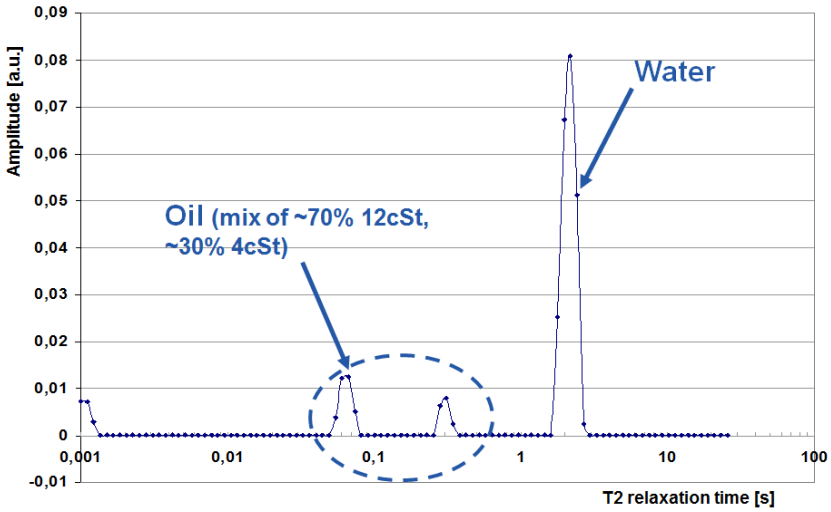

Figure 27 Example of a T_2 relaxation time spectrum analysis using prototype 1. There is a clear distinction between the MR relaxation times associated with water and oil. This analysis enables an estimation of the water-oil composition.

Two additional peaks were observed at 65 ms and 300 ms, respectively, corresponding to a viscosity of about 12 and 4cSt. Standard T_2-viscosity correlations have been used. According to this analysis, the oil sample under test is a composition of two oils (about 70% of 12 cSt oil and about 30% of 4cSt oil). This composition has subsequently been confirmed by the manufacturer of this oil. Besides typical flow metering applications, this specific example also illustrated the future potential of MR technology when considering additional diagnostic capabilities.

8. Summary and Conclusions

This paper describes the concept and industrialization of a magnetic resonance based multiphase flow meter. After introducing the magnetic resonance principle, its application to multiphase flow measurement has been described.
It is demonstrated that magnetic resonance technology enables a very elegant and direct way of measuring multiphase flow. In fact, it is the molecular flow of each individual phase that is being measured.
The capabilities of the magnetic resonance based multiphase flow meter has been demonstrated with two prototypes that have been extensively tested at various multiphase flow conditions.
The experimental data acquired during these measurements, show good performance of the flow meter across the entire application range with respect to the determination of both the gas volume fractions, water liquid ratio and the individual phase flow rates. In addition, data analysis shows that further improvements to the interpretation models are feasible. The improved models are expected to be available for the next series of tests.
While the magnetic resonance flow meter was found to work well across the entire application range, the experiments indicated that the meter is most sensitive for high water liquid ratio conditions (WLR>85%) in combination with lower gas volume fractions (GVF<75%). This sweet spot is in accordance with the theoretically expected performance.

In addition to multiphase flow metering capabilities, magnetic resonance offers many powerful diagnostic features with significant future potential. Some of these features have been illustrated in this paper.
An industrialized version of the MR multiphase flow meter is currently built. All options for improving the performance of the flow meter identified during three-phase flow tests in

commercial flow loops will be taken into consideration for this model. It is expected that the first industrial version of the magnetic resonance flow meter will be available for testing in various flow loops and oil field installations in the fourth quarter of 2013.

9. Acknowledgements

The authors of this paper like to express their appreciation to the entire MR development team and are particularly grateful to Marco Zoeteweij and Olaf Bousché from KROHNE for their contribution.

10. References

[1] M. Appel, *Nuclear Magnetic Resonance and Formation Porosity*, Petrophysics, Vol. 45, No.3, (May-June 2004); p296-307.

[2] M. Appel, et al., *Robust Multi-Phase Flow Measurement Using Magnetic Resonance Technology*, Society of Petroleum Engineers, MEOS, Manama, Bahrain, 6-9 March, 2011.

[3] Jankees Hogendoorn and Matthias Appel, *Magnetic Resonance for the Future; A New Methodology to Measure Multiphase Flow*, 4th International EMBT Conference, Hannover, 20.-21. March, 2013.

[4] G. Falcone, et al., *Multiphase Flow Metering, Principles and Applications*, Vol. 54, Developments in Petroleum Science, Elsevier, 2010.

[5] E. L. Hahn, *Spin Echoes*, Phys. Rev. 80 (1950) 580.

[6] P.T. Callaghan, *Principles of Nuclear Magnetic Resonance Microscopy*, Clarendon Press, Oxford, 1991.

[7] N. Bloembergen, E. M. Purcell, R. V. Pound, *Relaxation Effects in Nuclear Magnetic Resonance Absorption*, Phys. Rev. 73 (1948) 679-712.

[8] A. Abragam, *The Principles of Nuclear Magnetism*, Oxford University Press, New York, 599 p. (1961).

[9] Y. Zhang, et al.: *Oil and Gas NMR Properties: The Light and Heavy End*, 43rd Annual SPWLA Annual Logging Symposium, (June 2-5, 2002), Oiso, Japan, 2002.

[10] T.M. Osán, et al. : *Fast measurements of average flow velocity by Low-Field ^{1}H NMR*, Journal of Magnetic Resonance (1969) 209(2):7, 2011.

[11] *Handbook of Multiphase Flow Metering*, Norwegian Society for Oil and Gas Measurement, revision 2, March, 2005.